INTERNATIONAL JOURNAL FOR NUMERICAL METHODS IN FLUIDS, VOL. 5, 1017–1034 (1985)

A COUPLED SOLUTION OF THE VORTICITY–VELOCITY FORMULATION OF THE INCOMPRESSIBLE NAVIER–STOKES EQUATIONS

BAKHTIER FAROUK AND TORU FUSEGI

Department of Mechanical Engineering and Mechanics, Drexel University, Philadelphia, PA 19104, U.S.A.

SUMMARY

A relatively novel formulation of the Navier–Stokes equations is used for obtaining solutions of two dimensional incompressible fluid flow and convective heat transfer problems. A vorticity transport equation along with two Poisson equations for the velocity components and the energy equation are solved by a finite difference scheme. A coupled solution procedure is used for solving simultaneously the dependent variables along a line, using a block tridiagonal matrix algorithm. The formulation is found to be stable and has features that may be desirable for solving a wide variety of flow and heat transfer problems.

KEY WORDS: Vorticity–Velocity Numerical Method Coupled Solution Block Tridiagonal Matrix

INTRODUCTION

The vast majority of the numerical solutions of incompressible Navier–Stokes equations presented in the literature is based on the vorticity–stream function formulation. The vorticity–stream function formulation has the major advantages of avoiding the explicit appearance of the pressure and not having to solve the continuity equation directly. One of the major reasons for the success of the above formulation in predicting incompressible flow fields is that, by definition, the continuity equation is satisfied identically for all values of the stream function.[1] The stream function, by virtue of its definition, is valid for all two-dimensional flows, both rotational and irrotational. For steady flow vorticity–stream function formulations, an iteration scheme is usually introduced to handle the vorticity boundary condition at a solid surface. This iteration is in addition to the iteration required to solve the non-linear vorticity transport equation. In most of the published work to date, either point or line-by-line iteration schemes are employed where a sequential, 'one variable at a time' procedure is employed.[2]

The vorticity–stream function formulation, however, has serious limitations in calculating certain flows, e.g. in flows within multiply connected bodies or through flow passages, where the mass flow rates are not known *a priori*.[3,4] Also the calculation of vorticity at the solid walls requires the evaluation of a second-order derivative of the stream function at the wall. Since the early 1970's, there has been a noticeable shift of interest from the vorticity–stream function formulations of the Navier–Stokes equations to the primitive variable (u–v–p) formulations. Finite difference primitive variable formulations have been used with success by several investigators.[5–7] The primitive variable formulations for incompressible flows, however, suffer from the limitation that there is no obvious equation for obtaining the pressure field and there is no specified boundary condition for the pressure at the solid walls. The available methods for solving the primitive

0271–2091/85/121017–18$01.80

Received 19 March 1985
Revised 9 August 1985

variable formulation need considerable programming and storage effort (e.g. the use of staggered grids) and under-relaxation of the pressure-correction equation.

A relatively novel formulation of the Navier–Stokes equations employing the vorticity and velocity components for solving viscous incompressible fluid flow and heat transfer problems alleviates most of the drawbacks mentioned earlier for the vorticity–stream function and the primitive variables formulations. In addition, the vorticity–velocity formulation has easy application to higher-order accuracy difference methods and to non-orthogonal coordinate systems. The staggered grid used for the primitive variables formulation makes both difficult.

The vorticity–velocity formulation has been previously used by Fasel and coworkers[8–10] for hydrodynamic stability problems and by Fusegi and Farouk[11] for convective heat transfer problems. Caretto *et al.*[12] had used a mixed vorticity–velocity and primitive variable formulation to predict three-dimensional boundary layer flows. It has, however, been observed that the above formulation gives poor results when a sequential, 'one variable at a time' type iteration procedure is employed. This is particularly the case for high Reynolds or Rayleigh number flows. When point or line-by-line iteration schemes (with a sequential, 'one variable at a time' type approach) are employed, then the vorticity boundary conditions at solid walls lags the iteration cycle as the velocity values at the near wall nodes have to be obtained from the previous iteration. This drawback is eliminated in the coupled solution procedure employed here where the vorticity and velocity components (including the boundary values) are solved simultaneously along a given line.

The vorticity–velocity formulation evaluated in this paper solved by the coupled solution procedure has been found to be highly stable for a large range of Reynolds and Rayleigh numbers. These types of coupled solution procedures are quite common in aerodynamics, but have rarely been used for incompressible viscous flows.[13]

TEST PROBLEMS

In order to study the applicability of the formulation, fluid flow and heat transfer problems in a square cavity and horizontal circular annulus are considered as shown in Figures 1 and 2, respectively. For the square cavity, an insulated top (moving or stationary) wall is considered and the left and right vertical walls are maintained at constant temperatures. The bottom wall is also taken to be insulated. For the second geometry, the inner and outer cylinders are considered to be maintained at constant temperatures. Both stationary and rotating inner cylinders are considered.

The two geometries are chosen because a vast amount of results are available in the literature for fluid flow and heat transfer characteristics in the above cases (obtained either by the primitive variable or vorticity–stream function formulation), with which comparisons could be made with the results obtained from the present formulation and solution procedure.

Governing equations

The flow and heat transfer phenomena to be investigated here are described by the complete Navier–Stokes and energy equations for two-dimensional laminar incompressible flows. The viscous dissipation term in the energy equation is neglected and the Boussinesq approximation is invoked for the buoyancy induced body force term in the Navier–Stokes equations.

In the present formulation, the Navier–Stokes equations are expressed in the vorticity transport form (for the square cavity problem)

$$\frac{\partial \omega}{\partial t} + \frac{\partial}{\partial x}(u\omega) + \frac{\partial}{\partial y}(v\omega) = \frac{\partial}{\partial x}\left(\frac{\partial \omega}{\partial x}\right) + \frac{\partial}{\partial y}\left(\frac{\partial \omega}{\partial y}\right) + Gr\frac{\partial T}{\partial x}, \tag{1}$$

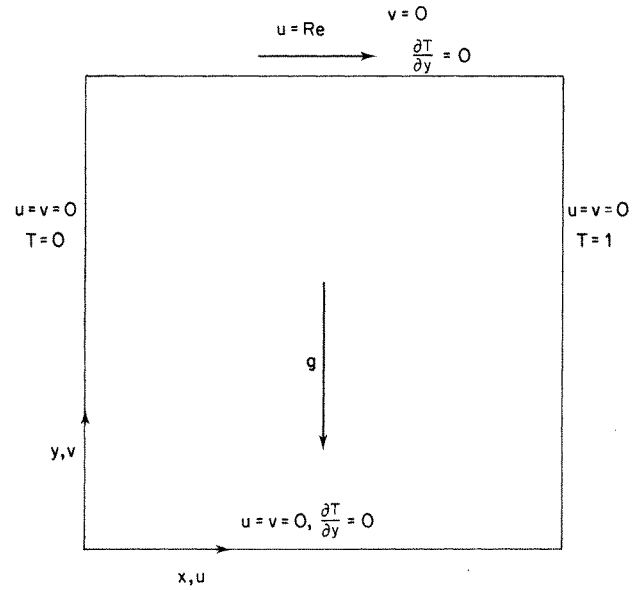

Figure 1. The geometry and the boundary conditions of the driven cavity problem and natural convection in the square cavity

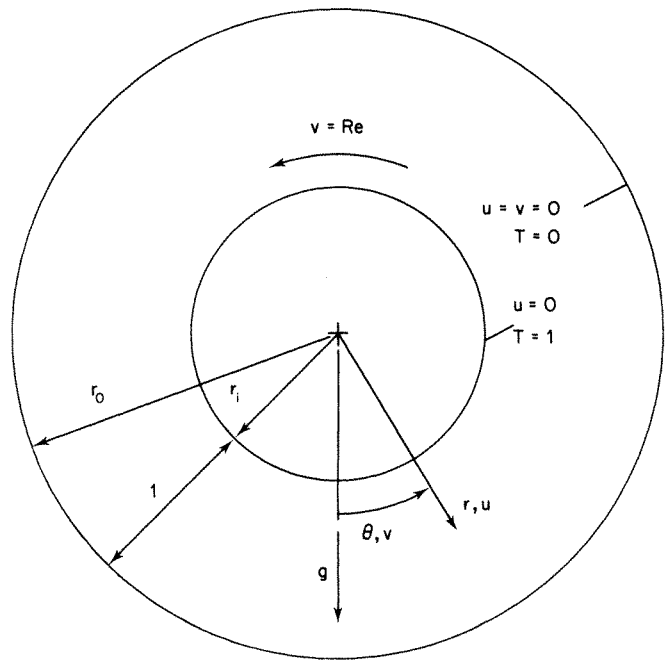

Figure 2. The geometry and the boundary conditions of natural and mixed convection in the annulus between the concentric cylinders

with the vorticity defined as

$$\omega = \frac{\partial v}{\partial x} - \frac{\partial u}{\partial y}, \tag{2}$$

and the continuity equation is given as

$$D = \frac{\partial u}{\partial x} + \frac{\partial v}{\partial y} = 0, \tag{3}$$

where the coordinate system is defined in Figure 1 for the Cartesian coordinates.

The two Poisson equations for the velocity components are given as

$$\frac{\partial^2 u}{\partial x^2} + \frac{\partial^2 u}{\partial y^2} = -\frac{\partial \omega}{\partial y} \tag{4}$$

and

$$\frac{\partial^2 v}{\partial x^2} + \frac{\partial^2 v}{\partial y^2} = \frac{\partial \omega}{\partial x}. \tag{5}$$

The energy equation is similar to the vorticity transport equation and can be expressed as

$$\frac{\partial T}{\partial t} + \frac{\partial}{\partial x}(uT) + \frac{\partial}{\partial y}(vT) = \frac{\partial}{\partial x}\left(\frac{1}{Pr}\frac{\partial T}{\partial x}\right) + \frac{\partial}{\partial y}\left(\frac{1}{Pr}\frac{\partial T}{\partial y}\right). \tag{6}$$

The two Poisson equations can be derived from the definition of vorticity, by differentiation with respect to y and x, respectively, and by making use of the continuity condition. Equations (1) along with equations (4)–(6) represent the governing equations in the vorticity–velocity formulation to study the incompressible viscous flow problems. For a given problem the above coupled equations system needs to be solved along with appropriate boundary conditions. The vorticity boundary conditions at the walls introduce additional coupling to the system.

The dependent variables above are given in non-dimensional forms and the variables are defined as follows:

$$x = \frac{x^*}{L}, \quad y = \frac{y^*}{L}, \quad u = \frac{u^* L}{\nu}, \quad v = \frac{v^* L}{\nu},$$

$$\omega = \frac{\omega^* L^2}{\nu}, \quad T = \frac{T^* - T_C}{T_H - T_C} \quad \text{and} \quad t = \frac{t^* \nu}{L^2},$$

where L is the characteristic length of the cavity and T_H and T_C are the right and left vertical wall temperatures, respectively.

For the concentric annulus problem the vorticity transport equation is given as

$$r\frac{\partial \omega}{\partial t} + \frac{\partial}{\partial r}(ru\omega) + \frac{\partial}{\partial \theta}(v\omega) = \frac{\partial}{\partial r}\left(r\frac{\partial \omega}{\partial r}\right) + \frac{\partial}{\partial \theta}\left(\frac{1}{r}\frac{\partial \omega}{\partial \theta}\right) + Gr\left(\frac{\partial T}{\partial \theta}\cos\theta + r\frac{\partial T}{\partial r}\sin\theta\right), \tag{7}$$

with the vorticity defined as

$$\omega = \frac{1}{r}\left\{\frac{\partial}{\partial r}(rv) - \frac{\partial u}{\partial \theta}\right\}, \tag{8}$$

and the continuity equation is given as

$$D = \frac{\partial}{\partial r}(ru) + \frac{\partial v}{\partial \theta} = 0,$$

where the coordinate system is defined in Figure 2.

The two Poisson equations in the cylindrical coordinate now become

$$\frac{\partial}{\partial r}\left(r\frac{\partial u}{\partial r}\right) + \frac{\partial}{\partial \theta}\left(\frac{1}{r}\frac{\partial u}{\partial \theta}\right) = -\frac{\partial \omega}{\partial \theta} - 2\frac{\partial u}{\partial r} - \frac{u}{r} \tag{9}$$

and

$$\frac{\partial}{\partial r}\left(r\frac{\partial v}{\partial r}\right) + \frac{\partial}{\partial \theta}\left(\frac{1}{r}\frac{\partial v}{\partial \theta}\right) = r\frac{\partial \omega}{\partial r} + 2\omega - 2\frac{\partial v}{\partial r} - \frac{v}{r}. \tag{10}$$

The energy equation can be expressed as

$$r\frac{\partial T}{\partial t} + \frac{\partial}{\partial r}(ruT) + \frac{\partial}{\partial \theta}(vT) = \frac{\partial}{\partial r}\left(\frac{1}{Pr}r\frac{\partial T}{\partial r}\right) + \frac{\partial}{\partial \theta}\left(\frac{1}{Pr}\frac{1}{r}\frac{\partial T}{\partial \theta}\right). \tag{11}$$

The dependent variables were non-dimensionalized as follows:

$$r = \frac{r^*}{L}, \quad u = \frac{u^* L}{\nu}, \quad v = \frac{v^* L}{\nu},$$

$$\omega = \frac{\omega^* L^2}{\nu}, \quad T = \frac{T^* - T_C}{T_H - T_C} \quad \text{and} \quad t = \frac{t^* \nu}{L^2},$$

where L is the gap width of the annulus and T_H and T_C are the inner and outer cylinder wall temperatures, respectively.

For the problem geometry as shown in Figure 1, the following boundary conditions are used:

$$u = 0, \quad v = 0, \quad \omega = \frac{\partial v}{\partial x}, \quad T = 0 \quad \text{at } x = 0, \quad 0 < y < 1,$$

$$u = 0, \quad v = 0, \quad \omega = \frac{\partial v}{\partial x}, \quad T = 1 \quad \text{at } x = 1, \quad 0 < y < 1,$$

$$u = 0, \quad v = 0, \quad \omega = -\frac{\partial u}{\partial y}, \frac{\partial T}{\partial y} = 0 \quad \text{at } 0 < x < 1, \quad y = 0,$$

and

$$u = Re, \quad v = 0, \quad \omega = -\frac{\partial u}{\partial y}, \frac{\partial T}{\partial y} = 0 \quad \text{at } 0 < x < 1, \; y = 1,$$

where the Reynolds number is given as $Re = UL/\nu$, U being the velocity of the moving wall.

For the problem geometry as shown in Figure 2, the following boundary conditions are specified:

$$u = 0, \quad v = Re, \quad \omega = \frac{1}{r}\frac{\partial}{\partial r}(rv), \quad T = 1 \quad \text{at } r = r_i, \quad 0 \leqslant \theta \leqslant 2\pi,$$

$$u = 0, \quad v = 0, \quad \omega = \frac{1}{r}\frac{\partial}{\partial r}(rv), \quad T = 0 \quad \text{at } r = r_o, \quad 0 \leqslant \theta \leqslant 2\pi,$$

where the rotational Reynolds number is given as $Re = r_i^* \Omega L/\nu$, Ω being the rotational speed of the inner cylinder.

SOLUTION METHOD

A coupled solution method (along a line) is presented here for solving the system of coupled differential equations via a block tridiagonal matrix algorithm. The set of governing equations is discretized by a control-volume-based finite difference method. The convective terms are approximated by a hybrid[14] differencing scheme and a fully implicit transient scheme is employed. It is seen that the vorticity and velocity equations are coupled and there is an additional coupling through the wall boundary conditions. However, the energy equation is coupled to the vorticity and velocity equations by the source term in the vorticity equation and the convection terms in the energy equation itself. The finite difference approximations to this set of flow equations must be solved iteratively. This is usually accomplished by the linearization process of employing the results of previous iteration in calculating the coefficients of the non-linear convective and source terms. In the present application of interest in the vorticity–velocity formulation, the difference equations are solved directly for a given line of grid points at constant x or constant r. The discretized system can be thought of as an ensemble of several tridiagonal subsystems coupled through diagonal submatrices. The system has the form

$$a^l_{i,j}\phi^l_{i,j-1} + b^l_{i,j}\phi^l_{i,j} + c^l_{i,j}\phi^l_{i,j+1} + \sum_{\substack{k=1 \\ k\neq l}}^{m} (a^k_{i,j}\phi^k_{i,j-1} + b^k_{i,j}\phi^k_{i,j} + c^k_{i,j}\phi^k_{i,j+1}) = e^l_{i,j} + f^l_{i,j}\phi^l_{0i,j}, \quad (12)$$

where the indices i and j represent spatial location and ϕ_0 denotes the values of ϕ at the previous time level. The above equation is written for each dependent variable ϕ^k $(k = 1, 2, \ldots m)$. The vorticity boundary conditions along the walls at constant x or r can also be cast into the above form. Second-order accurate finite difference expressions were used for the vorticity boundary conditions at the wall. The resulting equation system forms a block tridiagonal system. It is to be noted that along the given line all values of ϕ are considered at the same iteration level. The solution of the whole domain is obtained by sweeping along the y or θ directions. To accelerate convergence, the discretized equations can also be written along a given line of grid points at constant y or constant θ and the sweep directions are reversed. The reversing of sweep directions is especially important for the square cavity problem where walls are present along both constant x and constant y lines.

The iteration is terminated when values of the dependent variables at each grid point satisfy the following convergence criterion:

$$\max \left| (\theta^k_n - \theta^k_{n-1})/(\theta^k_n)_{\max} \right| \leqslant 10^{-5} \quad (k = 1, 2, \ldots, m),$$

where θ^k stands for any dependent variable and n the iteration level. The computations were carried out on a PRIME 850 computer. The approximate number of iterations required for convergence at each time level varies from 100 to 500, depending on the values of the Reynolds and Rayleigh numbers of the problem as well as on the number of grid points. Typical CPU times varied from thirty minutes to three hours.

RESULTS AND DISCUSSION

Results were obtained for forced and free convection problems in a square cavity and for free and mixed convection problems in the cylindrical annulus, using the vorticity–velocity formulation.

These results demonstrate the applicability of the vorticity–velocity formulation, which up to now has been ignored by the majority of investigators in convective heat transfer. The mixed convective problems considered in the cylindrical annulus are significant, as the problem is difficult to analyse in the vorticity–stream function formulation, due to the unknown mass flow rate through the cylindrical annulus.

Forced convection problems were solved first for the square cavity by setting $Gr = 0$ in the formulation, which decouples the energy equation from the vorticity transport and velocity equations. The driving force of the fluid motion is the sliding top in this case. This, so-called 'driven cavity', problem has been widely used by investigators to evaluate numerical schemes in the past.[15,16] Curiously, though the hydrodynamic problem has been solved by many researchers, no heat transfer results for the forced convection case could be found in the literature. Nusselt numbers for a similar problem have been reported by Chen *et al.*,[17] but different temperature boundary conditions were used in that case. Thus, for the forced convection problem, only flow characteristics obtained with the present formulation could be compared with previous studies.

For the forced convection, in the square cavity, results were obtained for the Reynolds number ranging from 10^0 to 10^3. Constant fluid properties with $Pr = 0{\cdot}721$ were used for all cases. A 51×51 uniform mesh was employed for the lower Reynolds number cases whereas a 51×51 non-uniform mesh was considered for the higher Reynolds numbers. The results obtained for lower Reynolds

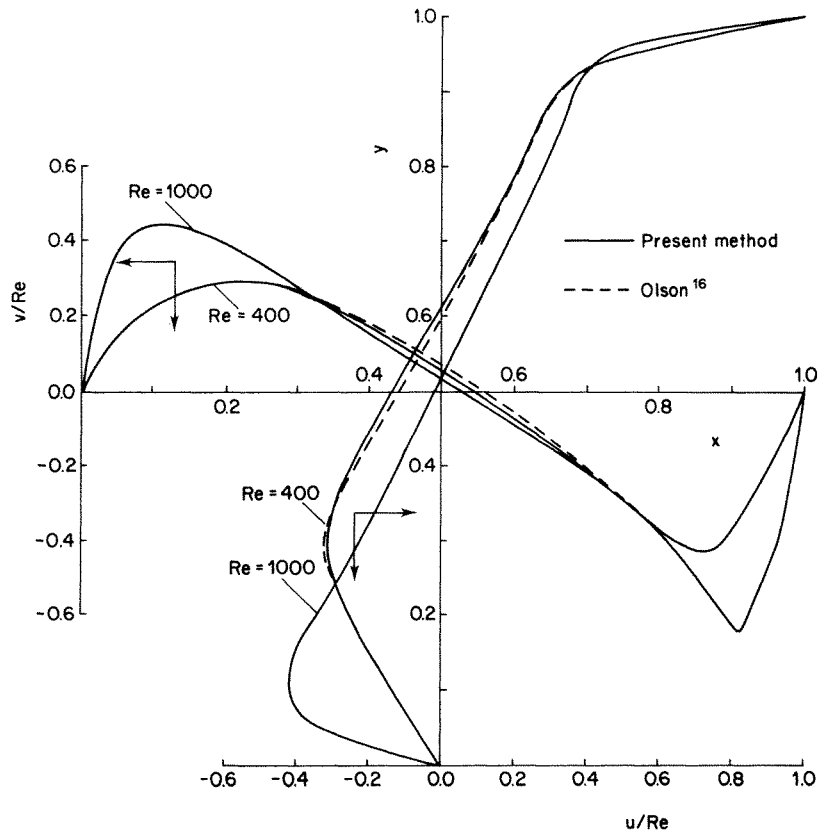

Figure 3. Profiles of u and v along the cavity vertical and horizontal mid-planes ($x = 0{\cdot}5$ and $y = 0{\cdot}5$, respectively) for different moving lid velocities (Re) ($Ra = 0$)

number cases were used as the initial data of the computation for higher Reynolds number cases. No under-relaxation factor is used for the forced convection studies.

Figure 3 shows the u velocity distributions at the cavity vertical mid-plane ($x = 0{\cdot}5$) and v profiles at the horizontal mid-plane ($y = 0{\cdot}5$) for $Re = 400$ and 1000. For lower Reynolds numbers (not shown here) the predictions had excellent agreement with previous studies.[18] The u and v profiles at the vertical and horizontal mid-planes, respectively, at $Re = 400$ are compared with the solutions given by Olson[16] in Figure 3. Very good agreements are obtained in this case. No numerical instabilities were observed in the solution procedure.

Figure 4 gives the streamlines (ψ/Re) computed from the velocity field at $Re = 1000$. The results are in good qualitative agreement with the predictions given by de Vahl Davis and Mallinson.[19] The temperature results in this case could not be compared with previous studies owing to the lack of the same geometry with similar temperature boundary conditions in the literature. It was, however, observed that a very large temperature gradient occurs near the hot wall as the Reynolds number increases. The local Nusselt number at the hot vertical wall remains fairly uniform for most of the length and then increases rapidly as the moving lid is approached. The cold wall characteristics are different and the Nusselt number peaks only at the middle in this case.

Free convection results in the cavity are presented next, obtained by the vorticity–velocity formulation. The top wall was considered to be stationary and the fluid motion is caused solely by the buoyancy effects. The Rayleigh number was varied from 10^2 to 10^6 and a constant Prandtl number of 0·721 was used. A 31 × 31 mesh was used for the lower Rayleigh numbers and it was

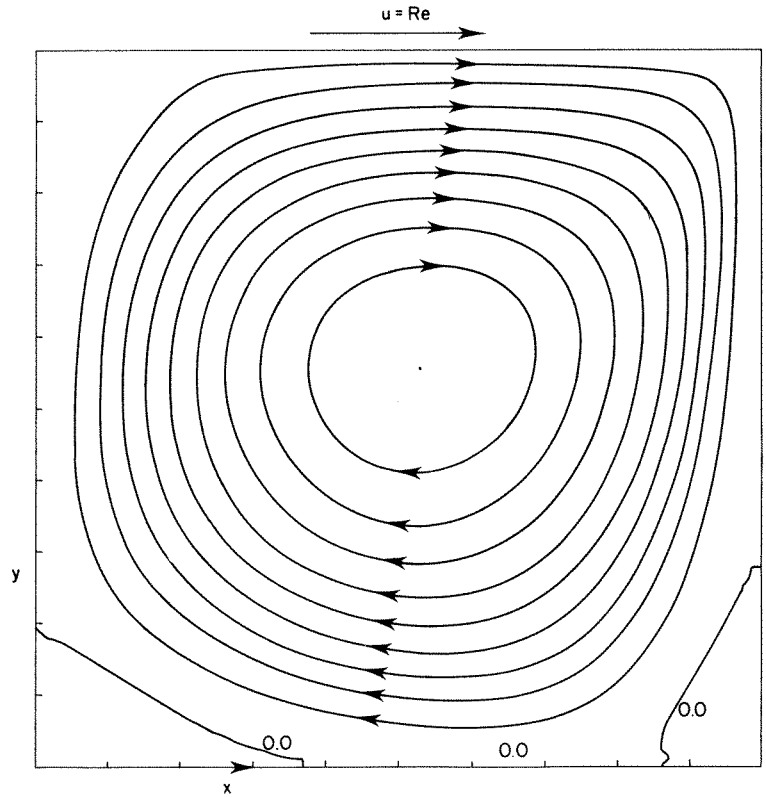

Figure 4. Stream function (ψ/Re) contours at $Re = 1000$ ($\Delta(\psi/Re) = 0{\cdot}0142$) ($Ra = 0$)

gradually increased to a 65 × 65 mesh for the highest Rayleigh number studied. For the higher Rayleigh number cases, a non-uniform mesh was employed owing to the formation of boundary layers.

The natural convection results were compared with a recent bench mark numerical solution of the same problem by de Vahl Davis.[20] In general, the agreements of the present solution obtained by the vorticity–velocity formulation with those given in Reference 20 are excellent.

The u and v profiles at the vertical and horizontal mid-sections are shown in Figure 5 for $Ra = 10^4$. The profiles are symmetric and the location and magnitude of the maximum values of u and v as given in Reference 20 are also shown in Figure 5. The agreement appears to be very good. With higher Rayleigh numbers, the velocity peaks move closer to the walls, indicating formation of boundary layers.

The isotherms are presented for $Ra = 10^4$, 10^5 and 10^6 in Figures 6, 7 and 8, respectively. In all cases shown the isotherms are found to undergo an inversion at the central region of the cavity. The formation of the thermal boundary layers along the cold and hot walls is clearly observed as Ra increases. At $Ra = 10^6$, the fluid is thermally stratified except for the thermal boundary layer regions near the vertical walls. The present prediction show good qualitative agreement with the solution in Reference 20.

The local Nusselt number distribution at the cold and hot walls for various Rayleigh numbers is shown in Figure 9.

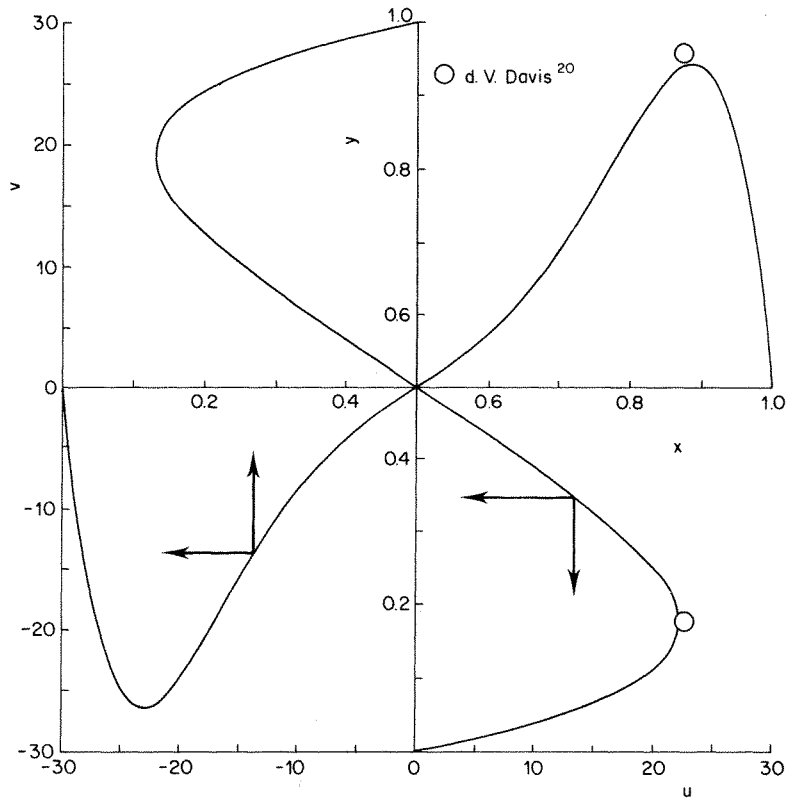

Figure 5. Profiles of u and v along the cavity vertical and horizontal mid-planes ($x = 0{\cdot}5$ and $y = 0{\cdot}5$, respectively) with $Ra = 10^4$

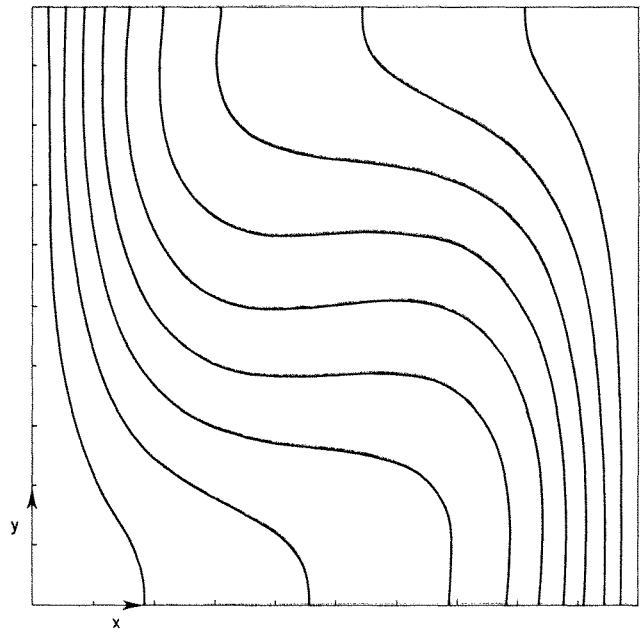

Figure 6. Isotherms (T) at $Ra = 10^4$ ($\Delta T = 0{\cdot}1$) (natural convection)

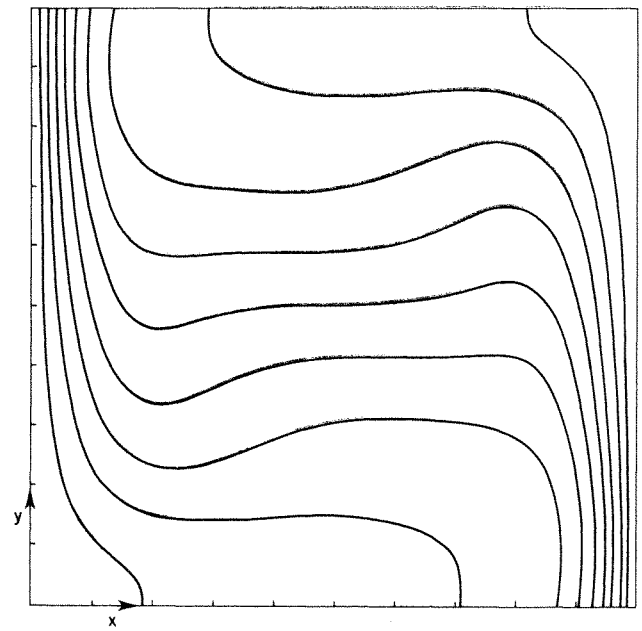

Figure 7. Isotherms (T) at $Ra = 10^5$ ($\Delta T = 0{\cdot}1$) (natural convection)

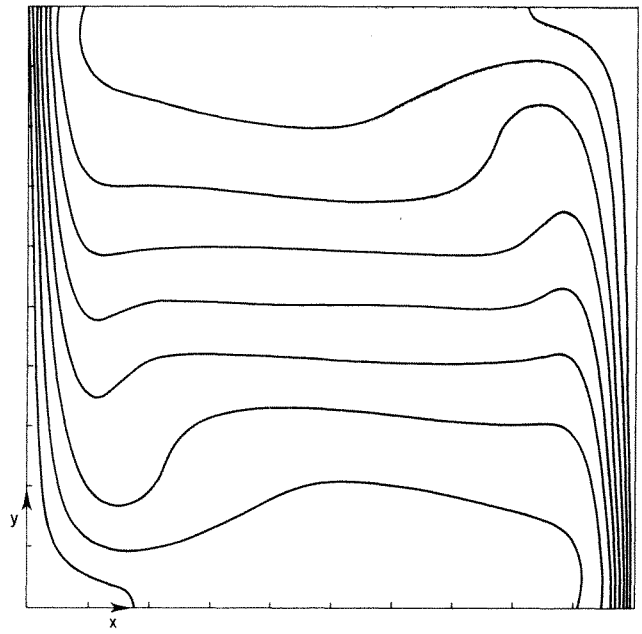

Figure 8. Isotherms (T) at $Ra = 10^6$ ($\Delta T = 0{\cdot}1$) (natural convection)

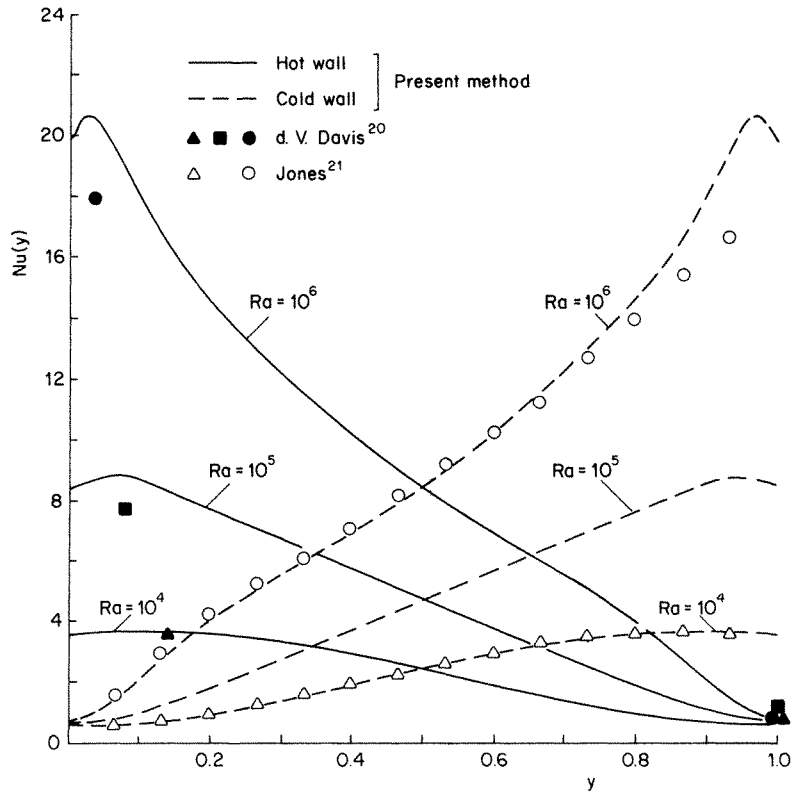

Figure 9. Distribution of the local Nusselt number ($Nu(y)$) along the cavity cold and hot walls ($x = 0$ and $x = 1$, respectively) for various Ra (natural convection)

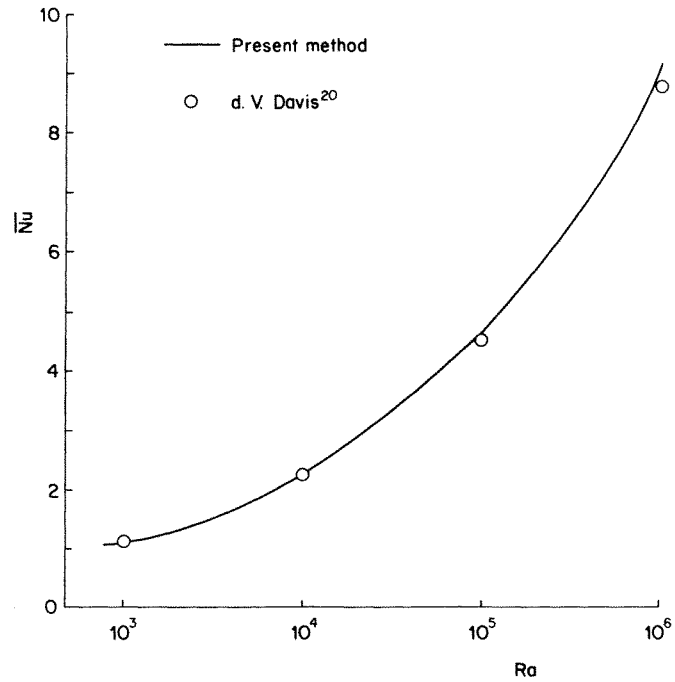

Figure 10. Change in the average Nusselt number ($\overline{Nu}$) with Ra (natural convection)

The location and magnitude of the maximum Nusselt numbers at different Rayleigh numbers as given in Reference 20 are also shown in the figure. The solutions given by Jones[21] at $Ra = 10^4$ and 10^6 are also compared with the present solutions and the agreement is found to be good.

The mean Nusselt number predictions are compared with those given in Reference 20 in Figure 10. The predictions almost overlapped with the solution given in Reference 20. No solutions above $Ra = 10^6$ were attempted as the flow may no longer be laminar and stable in those cases.

Natural convection in the annulus between the concentric cylinders is investigated next. The geometry of the problem is shown in Figure 2. The ratio of the gap width, L, to the inner cylinder diameter, $2r_i$, is held fixed at 0·8. The stationary inner cylinder is considered first. The direction of the gravitational force is taken as $\theta = 0°$. Values of θ increase counterclockwise from that direction. The Rayleigh number defined with the gap width, L, and the temperature difference of the cylinder surface, $T_H - T_C$, was varied from 10^2 to 10^5. Beyond the maximum Ra studied, the flow is thought to become turbulent.[22] The Prandtl number was set at a constant value, 0·721. The entire domain of the annulus was solved without considering symmetry planes for obtaining greater numerical accuracy. The number of grid points used for the computation was 41 in the r direction and 72 in the θ direction. At Rayleigh numbers over 10^4, non-uniform grids were used. Finer grids distributed near the cylinder surfaces can handle fine structures of flow motion and heat transfer phenomena, namely, the formation of the boundary layers and that of the plumes. To compute higher Ra cases, solutions for lower Ra are used as the initial guesses of the iterative solution procedure, as before. No under-relaxation was necessary for all cases studied.

Solutions were compared with the numerical results by Kuehn and Goldstein ($Pr = 0·70$)[22] whenever possible and showed excellent agreement.

Figure 11 shows the profiles of v along the horizontal plane ($\theta = 90°$) for various Ra. The solutions for $\theta = 270°$ were exactly symmetric with the presented results about $v = 0$. For a small

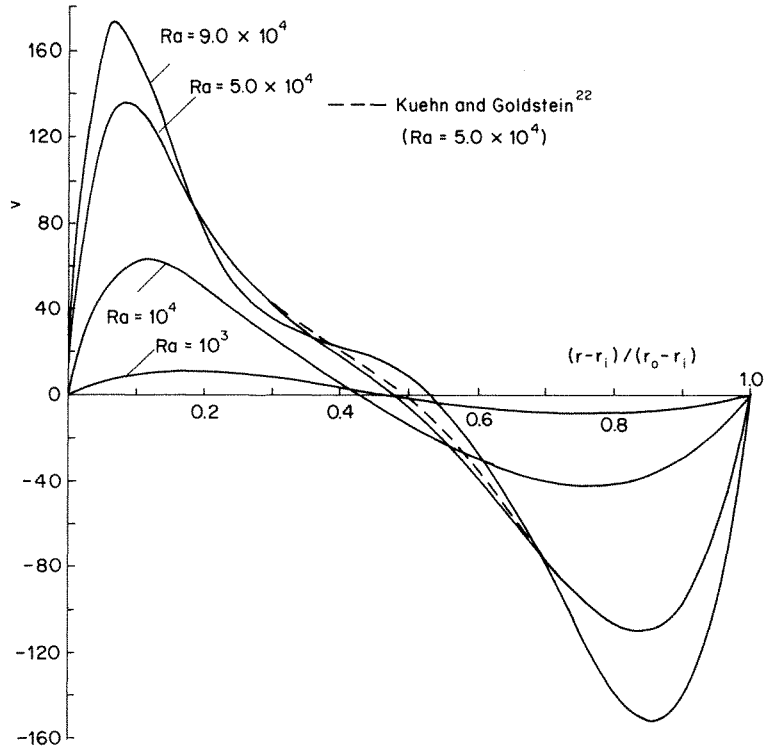

Figure 11. Profiles of v at the horizontal plane ($\theta = 90°$) for various Ra for the annulus problem (natural convection)

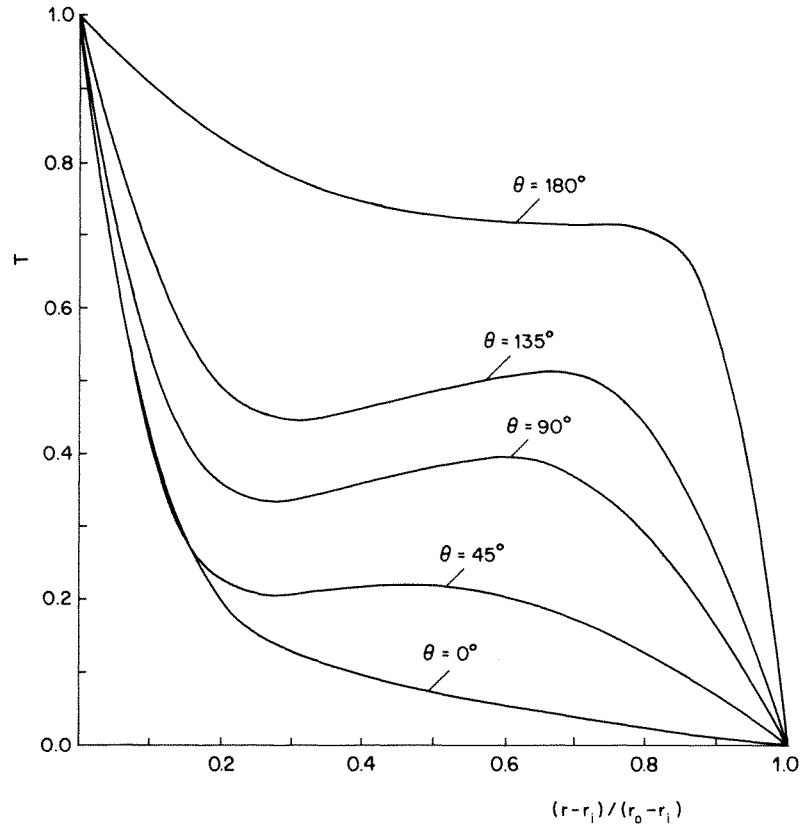

Figure 12. Profiles of temperature (T) along planes of constant values of θ at $Ra = 5 \times 10^4$ (natural convection)

Rayleigh number ($Ra = 10^3$), the profile is almost axisymmetric about the mid-point of the gap. As the Rayleigh number increases, the locations where the maximum and minimum values of v occur approach the cylinder walls and the velocity profile forms steeper slopes, indicating the formation of the boundary layers. The results at $Ra = 5 \times 10^4$ almost overlap with the solution in Reference 22.

Radial profiles of the temperature along different θ lines are shown in Figure 12 for $Ra = 5 \times 10^4$. Sharp temperature gradients are obtained for the inner cylinder at lower values of θ. For the outer cylinder heat transfer is high at the top region where the plume arising from the inner cylinder impinges on the outer cylinder. The predictions agreed well with the solutions given by Kuehn and Goldstein.[22]

The distribution of the local equivalent conductivity, λ, on the cylinder surfaces is shown in Figure 13. The equivalent conductivity is defined as the actual heat flux divided by the heat flux that would occur by pure conduction in the absence of fluid motion. For the inner cylinder, the location where the maximum equivalent conductivity occurs is at the bottom stagnation point and that of the minimum value is at the top stagnation point. At $Ra = 10^3$, the curves for both the inner and outer cylinders lay about $\lambda = 1$, which indicates that heat transfer is in the conduction regime. However, for over $Ra = 5 \times 10^4$, sharp peaks of λ appear at the top region of the outer cylinder owing to the impinging plume.

The results in Reference 22 are also plotted in the figure and show good agreement with the present prediction.

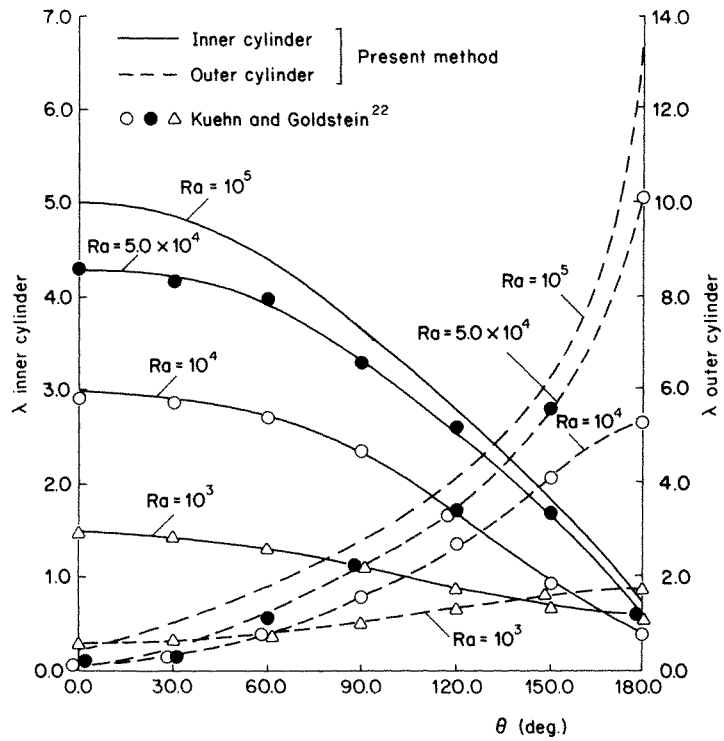

Figure 13. Distributions of the local equivalent conductivity (λ) on the inner and outer cylinder surfaces for various Ra (natural convection)

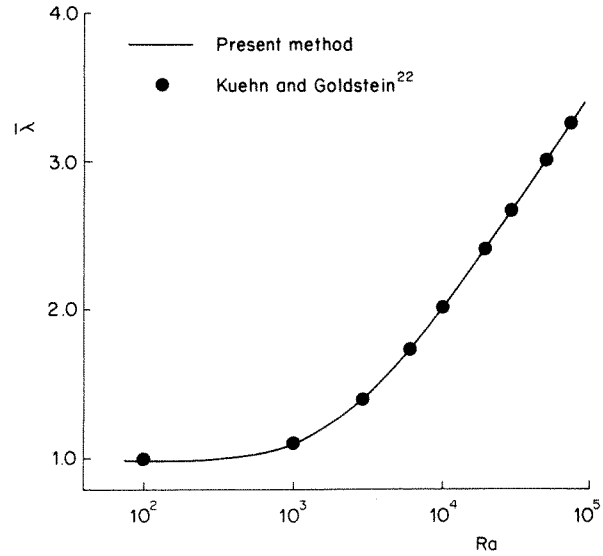

Figure 14. Change in the average equivalent conductivity ($\bar{\lambda}$) with Ra (natural convection)

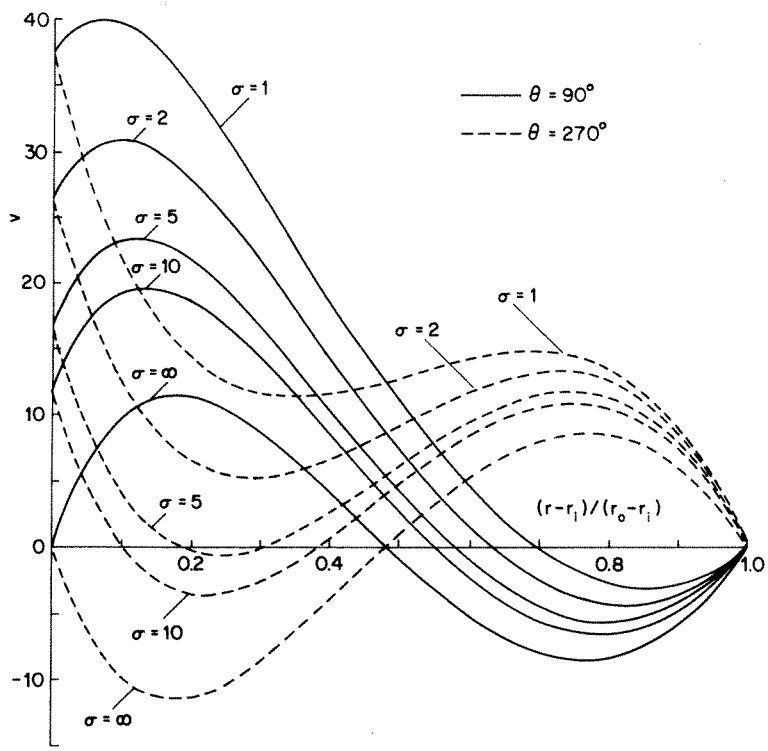

Figure 15. Angular velocity distributions for the annulus with rotating inner cylinder at $Ra = 10^3$

Figure 14 represents the change in the average equivalent conductivity with increasing Rayleigh numbers. It is observed from the figure that up to Ra approximately 10^3, heat transfer is almost solely due to conduction. Over $Ra = 6 \times 10^3$. $\bar{\lambda}$ increases linearly with the logarithm of Ra. The prediction by Reference 22 falls on the curve produced by the present study over the entire range of Rayleigh numbers investigated.

Finally, results for mixed convective flows in an annulus are presented where the heated inner cylinder is rotating. The net flow rate through the annulus is not known *a priori* for various combinations of the Grashof and rotational Reynolds number. The vorticity–stream function formulation is unsuitable for problems of this class.[23] The vorticity–velocity formulation along with the block tridiagonal matrix algorithm was found to give good results in this case. It can be shown that the parameter $\sigma = Gr/Re^2$ determines the relative strength of effects of the buoyancy and the centrifugal forces in the above problem. The pure natural convective flows reported earlier correspond to the case $\sigma = \infty$. Figure 15 displays the radial angular velocity profiles for $Gr = 1{\cdot}39 \times 10^3$ ($Ra = 10^3$) with varying values of σ. The inner cylinder is considered to be rotating counterclockwise and the results are shown for $\theta = 90°$ (the ascending side) and $\theta = 270°$ (the descending side). For the ascending side buoyancy enhances the rotation induced flow and suppresses the flow in the descending side. The average equivalent conductivities were found to decrease slightly for decreasing values of σ. This is because the rate of growth of the thermal boundary layer on the ascending side of the inner cylinder is less rapid than on the descending side. It is conjectured that the interaction seen between the buoyant and centrifugal effects could delay the transition to the Taylor-vortex flow.[24] This, however, needs further careful studies.

CONCLUSION

The study has successfully demonstrated the applicability of the vorticity–velocity formulation in solving a variety of fluid flow and heat transfer problems in different geometries. A coupled solution procedure is used for solving simultaneously (instead of the traditional 'one variable at a time' approach) along a line using a block tridiagonal matrix algorithm. The formulation also allows relatively easy extension to full three dimensions where six dependent variables (for the Navier–Stokes equations) are required. With the advent of powerful computers, the problem of storage requirement has lessened and the formulation may be attractive owing to its other advantages.

ACKNOWLEDGEMENT

This material is based upon work supported by the National Science Foundation under Grant No. MEA–83075606.

APPENDIX

Nomenclature

a, b, c, e, f	elements of the block tridiagonal matrix system of the finite difference equations
g	acceleration due to gravity
Gr	Grashof number
L	cavity length; gap width of the concentric cylinder
$Nu(y)$	local Nusselt number at y
Nu	average Nusselt number
Pr	Prandtl number

r	radial coordinate
Re	Reynolds number
t	time
T	temperature
T_C	cold wall temperature
T_H	hot wall temperature
u, v	velocity components in the x and y directions, respectively, in the Cartesian coordinate system; velocity components in the r and θ directions, respectively, in the polar coordinate system
U	velocity of the moving lid
x, y	horizontal and vertical coordinates, respectively

Greek letters

θ	circumferential coordinate
$\lambda(\theta)$	local equivalent conductivity at θ
$\bar{\lambda}$	average equivalent conductivity
ν	kinematic viscosity of fluid
ϕ	a dependent variable
ϕ_0	value of ϕ at the previous time level
σ	parameter to indicate the relative strength of effects of the buoyancy and the centrifugal forces ($= Gr/Re^2$)
ψ	stream function
ω	vorticity
Ω	rotational speed of the inner cylinder

Subscripts

i, j	location of the associated elements in the block matrix system

Superscripts

k, l, m, n	indices for dependent variables
*	dimensional value

REFERENCES

1. I. G. Currie, *Fundamental Mechanics of Fluids*, McGraw-Hill, New York, 1974.
2. A. D. Gosman, W. M. Pun, A. K. Runchal, D. B. Spalding and M. Wolfshtein, *Heat and Mass Transfer in Recirculating Flows*, Academic Press, New York, 1969.
3. M. D. Gunzburger and J. S. Peterson,'On the finite element approximation of the stream function-vorticity equations', *Advances in Computer Methods for Partial Differential Equations V*, R. Vichnevetsky and R. S. Stepleman (eds.), IMACS, 47–56, 1984.
4. B. Farouk and S. I. Guceri, 'Natural convection from a horizontal cylinder within confining walls', *Numerical Heat Transfer* **5**, 324–341 (1982).
5. S. V. Patankar and D. B. Spalding, 'A calculation procedure for heat and mass transfer in three-dimensional parabolic flows', *Int. Journal Heat Mass Transfer* **15**, 1787–1806 (1972).
6. W. R. Briley and H. McDonald, 'Analysis and computation of viscous subsonic primary and secondary Flows', *AIAA Paper 79–1453*, 1979.
7. K. N. Ghia and J. S. Sokhey, 'Laminar incompressible viscous flow in curved ducts of rectangular cross-sections', *J. Fluids Engineering* **99**, 640–645 (1977).

8. H. F. Fasel, 'Investigation of the stability of boundary layers by a finite-difference model of the Navier–Stokes equations', *J. Fluid Mechanics* **78,** 355–383 (1976).
9. H. Fasel and O. Booz, 'Numerical investigation of supercritical Taylor-vortex flow for a wide Gap', *J. Fluid Mechanics* **138,** 21–52 (1984).
10. H. Fasel, H. Bestek and R. Schefenacher, 'Numerical simulation studies of transition phenomena in incompressible two-dimensional flows', *Proc. AGARD Conf. on Laminar-Turbulent Transition*, Lyngby, Denmark, 1977, AGARD-CP-224, *Paper No. 14.*
11. T. Fusegi and B. Farouk, 'On the vorticity–velocity formulation of the Navier–Stokes equations for solving fluid flow and heat transfer problems', *ASME/AIChE National Heat Transfer Conference*, Denver, Colorado, 85-HT-8, August 1985.
12. L. S. Caretto, R. M. Curr and D. B. Spalding, 'Two numerical methods for three-dimensional boundary Layers', *Computer Methods in Applied Mechanics and Engineering* **1,** 39–57 (1972).
13. D. A. Anderson, J. C. Tannehil and R. H. Pletcher, *Computational Fluid Mechanics and Heat Transfer*, McGraw-Hill, New York, 1983.
14. S. V. Patankar, *Numerical Heat Transfer and Fluid Flow*, Hemisphere Publishing, Washington, D.C., 1980.
15. S. G. Rubin *et al.*, 'Numerical studies of incompressible viscous flow in a driven cavity', *NASA, SP-378*, 1975.
16. M. D. Olson, 'Comparison problem no. 1, recirculating flow in a square cavity', University of British Columbia, Civil Engineering, *Structural Research Series Report No. 22*, 1979.
17. C. J. Chen, H. Naseri-Neshat and K. S. Ko, 'Finite analytic solution of heat transfer in two dimensional cavity flow', *Numerical Heat Transfer* **4,** 179–197 (1981).
18. O. R. Burggraf, 'Analytical and numerical studies of the structure of steady separated flows', *J. Fluid Mechanics* **24,** 113–151 (1966).
19. G. de Vahl Davis and G. D. Mallinson, 'An evaluation of unwind and central difference approximations by a study of recirculating flow', *Computers and Fluids* **4,** 29–43 (1976).
20. G. de Vahl Davis, 'Natural convection of air in a square cavity: a bench mark numerical solution', *Int. j. numer. methods fluids* **3,** 249–264 (1983).
21. I. P. Jones, 'A comparison problem for numerical methods in fluid dynamics, the "double glazing problem"', in R. W. Lewis and K. Morgan (eds.) *Numerical Methods in Thermal Problems*, Pineridge Press, Swansea, U.K., 1979, pp. 338–348.
22. T. H. Kuehn and R. J. Goldstein, 'An experimental and theoretical study of natural convection in the annulus between horizontal concentric cylinders', *J. Fluid Mechanics* **74,** 695–719 (1976).
23. K. S. Ball and B. Farouk, 'Laminar mixed convection in the annulus between horizontal concentric cylinders with rotating inner cylinder', *Advances in Computer Methods for Partial Differential Equations V*, R. Vichnevetsky and R. S. Stepleman (eds.), IMACS, 80–83, 1984.
24. G. I. Taylor, 'Stability of a viscous liquid contained between two rotating cylinders', *Phil. Trans. Roy. Soc. A* **223,** 289–343 (1923).